Simulative investigation of microcylinder-assisted microscopy in reflection and transmission mode

Tobias Pahl[a], Sebastian Hagemeier[a], Lucie Hüser[a], Felix Rosenthal[a], and Peter Lehmann[a]

[a]Measurement Technology Group, Faculty of Electrical Engineering and Computer Science, University of Kassel, Wilhelmshöher Allee 71, 34109 Kassel, Germany

ABSTRACT

Microsphere and microcylinder-assisted microscopy (MAM) has grown to an intensively studied optical far-field imaging technique over the last decade that overcomes the fundamental lateral resolution limit of a given microscope. However, the physical effects leading to resolution enhancement are still frequently debated. In addition, various configurations of MAMs operating in transmission as well as reflection mode are examined and results generalized. We present a rigorous simulation model of MAM and present a way to quantify the resolution simulatively. The lateral resolution is compared for microscope arrangements in reflection and transmission mode. Further, we discuss different physical effects with respect to their contribution to resolution enhancement. The results indicate that the effects affecting the resolution as well as the enhancement itself strongly depend on the arrangement of the microscope and the measurement object.

Keywords: microsphere-assisted microscopy, resolution enhancement, resolution limit, electromagnetic modeling

1. INTRODUCTION

Optical microscopy is one of the most widely used imaging techniques in science and industry with various fields of application. Due to the wave properties of light and resulting diffraction effects, conventional optical microscopes operating in the far-field are subject to the fundamental lateral resolution limit. According to Abbe, the minimum resolvable period length l_x of a periodic measurement object is given by $l_x = \lambda/(2\mathrm{NA})$ with the light wavelength λ and the numerical aperture (NA) of the microscope objective lens.[1]

In order to overcome this fundamental resolution limit, several optical measurement techniques have been developed based on near- as well as far-field detection of light fields. For an overview of existing methods overcoming or bypassing the resolution limit, we refer to Huszka and Gijs.[2]

One of the most promising and simple methods to enhance the resolution is placing microelements such as solid immersion lenses (SILs),[3,4] microspheres[5,6] or -cylinders[7,8] in the measurement object's near-field. Due to its simplicity and resolution improvement using a setup still operating in the far-field and hence remaining fast and contactless, microsphere and -cylinder-assisted microscopy (MAM) is part of various experimental and theoretical studies of the last decade. Since there are many publications addressing MAM and a detailed overview is out of the scope of this paper, we just list a few and e.g. refer to Wang and Luk'yanchuk[9] or Darafsheh[10] for more insights. Generally, it should be mentioned that microspheres are usually applied in experimental studies due to the resolution enhancement in both lateral directions, whereas microcylinders are more often considered in theoretical studies for computational reasons. Further, MAM can be combined with other techniques such as confocal,[11,12] interference[13–15] or fluorescence microscopy[16,17] to enhance the lateral or axial resolution.

Despite many investigations, the major reason for the obtained resolution enhancement is not clearly clarified yet. However, evanescent waves (EWs),[18,19] photonic nanojets (PNs),[5,20] whispering-gallery modes (WGMs)[21,22] and super-resonances[23] are effects frequently mentioned in the context of MAM. A detailed overview of optical phenomena occurring in microelements is provided by Minin and Minin.[24] Other recent studies come to the conclusion that the resolution enhancement mainly results from a local increase of the effective NA.[10,25–27] This result is in agreement with the observation that the point spread function of a microelement is a more accurate

Further author information: (Send correspondence to Tobias Pahl)
Tobias Pahl: E-mail: tobias.pahl@uni-kassel.de

indicator for resolution compared to the PN.[28]
In order to analyze the imaging properties of microelements and study influences of several phenomena potentially contributing to resolution enhancement, several numerical models are developed.[26,29–31] However, a full modeling of MAM including conical illumination and detection, considering coherence effects as well as a rigorous treatment of the scattering process is until recently missing.[9] In a recent study,[26] we present such a full modeling of microcylinder-assisted interference microscopy based on the theory published elsewhere.[32,33] We found that the local NA increase due to the microelement is the most likely reason for the resolution enhancement. Further, the enhanced resolution is independent of the NA of the objective lens. This observation is in good agreement to measurement results obtained by Duocastella et al.[25]
Nonetheless, the results obtained so far hold for imaging phase objects in reflection mode. However, the imaging of objects modulating the amplitude of the electric field referred to as amplitude objects, where e.g. other types of evanescent waves occur, plays an important role in conventional MAM. Further, MAM can operate in transmission as well as reflection mode.[9]
In order to analyze the resolution enhancement for both, microscopes that operate in reflection or transmission mode, the model[26] is extended to MAM of amplitude objects. In case of transmission, the microcylinder is used for either illumination or imaging only. Hence, we compare three different configurations to obtain a deeper understanding of the imaging properties in MAM.

2. SETUP AND MODELING

This section briefly describes the microscopic setup and the modeling used in this study. Figure 1(a) displays a schematic representation of an exemplary microcylinder-assisted microscope in reflection mode. The illumination beam path is shown in red and the imaging beam path in blue. A diffuser illuminated by an LED represents a homogeneous, spatially extended light source, which is imaged in the back focal plane of the microscope objective. Later in this paper we consider solely a vertically incident plane wave for illumination corresponding to a point light source instead of the diffuser leading to a reduced illumination NA and thus a reduced computation time. However, the resolution enhancement achieved using a microcylinder is independent of the illumination NA as shown elsewhere.[26]
The microcylinder (radius $r = 2.5\,\mu\text{m}$, refractive index $n = 1.5$) is placed directly above an amplitude grating consisting of glass ($n = 1.5$) and aluminum. The light-surface interaction of the incident light with the measurement object is simulated using the finite element method (FEM). Figure 1(b) shows the geometry of the FEM setup, where the microcylinder surrounded by air is placed on an amplitude grating of finite or infinite thickness and period length l_x. The top and the bottom boundaries of the geometry are extended by so called perfectly matched layers (PMLs), which damp the scattered field exponentially to zero without reflections at interfaces to artificially constitute the case of an infinitely extended space. Laterally, the geometry is assumed to be periodic with period length $L_x = 13.2\,\mu\text{m}$ considered in the modeling by quasi-periodic boundary conditions. For more information and explanation on the modeling we refer to previous studies.[26,32] The incident wave, which is considered by appropriate boundary conditions for the electric field $\mathbf{E}_{\text{top}}$ at the top and $\mathbf{E}_{\text{bottom}}$ at the bottom boundary, can be chosen to propagate from the top to the bottom boundary or vice versa depending on the microscope configuration.
In this study, we compare the achievable resolution enhancement for three different microscope configurations sketched in Fig. 1(c). In the first case (left figure), which corresponds to the setup shown in Fig. 1(a), the microscope operates in reflection mode. Hence, the microcylinder affects both, the illumination as well as the imaging beam path. The other two configurations correspond to the transmission mode, where the microcylinder is solely used for either imaging (middle figure) or illumination (right figure). Therefore, we analyze the influence of the microcylinder on the illumination and the imaging process separately.
Figure 2 presents extracts of simulated intensities for vertically incident plane waves computed for TE ((a-c), wavelength $\lambda = 448.975\,\text{nm}$) and TM ((d-f), $\lambda = 442.951\,\text{nm}$) polarization in reflection (a, b, d, e) and transmission (c, f). The illumination wavelength is chosen to excite a WGM for both polarization states since WGMs are frequently mentioned in context with resolution enhancement in MAM. For TE the refractive index of aluminum is given by $n = 0.389 + 4.287\text{i}$, for TM $n = 0.379 + 4.228\text{i}$.[34] In all figures the intensity of the total field, which equals the sum of the incident and scattered field, is shown.
In order to analyze the influence of the thickness d of the amplitude object, the simulations in reflection mode are

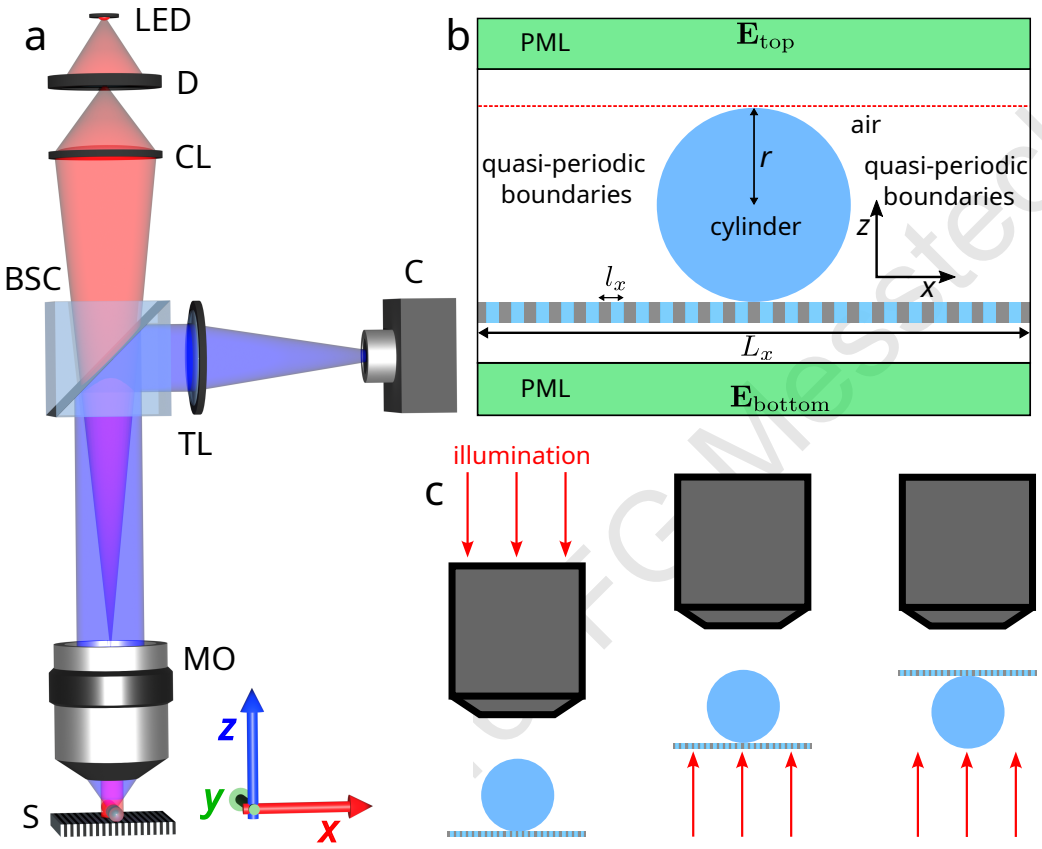

Figure 1. (a) Schematic representation of an exemplary microcylinder-assisted microscope in reflection mode with LED illumination, diffuser (D), condenser lens (CL) beam splitter cube (BSC), tube lens (TL), camera (C), microscope objective (MO) and sample with microcylinder placed on (S). The spatially incoherent Köhler illumination is sketched in red, the imaging beam path is shown in blue. (b) Geometry of the FEM setup including the microcylinder of radius r placed on an amplitude grating of period length l_x. The whole geometry is assumed to be periodic with period length L_x and, hence, quasi-periodic boundary conditions are considered for the left and right boundaries. To avoid reflections, the simulation area is extended by absorbing layers called perfectly matched layer (PML) on the top and the bottom of the geometry. The incident wave can be chosen to propagate from $\mathbf{E}_{\text{top}}$ to $\mathbf{E}_{\text{bottom}}$ or vice versa to consider microscope setups in reflection as well as transmission mode. In case of an axially infinitely extended measurement object, the grating ends in the PML, whereby the PML is implemented as a grating as well. The far-field is calculated based on the scattered field obtained at the red dotted line closely above the cylinder or closely below the measurement object, approximately where L_x is marked in the figure. (c) Three different microscope configurations where the red arrows specify the direction of the illumination. The left figure shows the setup in reflection mode corresponding to the setup sketched in (a), where the cylinder affects both, the illumination and the imaging beam path. The middle and right figures display the case of transmission mode with the cylinder in the imaging (middle) or illumination (right) beam path.

performed for a grating of infinite (Fig. 2(a), 2(d)) and finite thickness of $d = 100\,\text{nm}$ (Fig. 2(b), 2(e)). Comparing Fig. 2(a) to Fig. 2(b) and Fig. 2(d) to Fig. 2(e), the fields especially inside the cylinder differ depending on the thickness of the grating. Hence, internal reflections from the bottom of the grating and eventually evanescent waves occurring at the interface between the grating and air seem to have an impact. Thus, we compare results for both, infinite and finite thickness, in this study. Further, placing the cylinder below the grating instead of above strongly affects the fields, since in this case the cylinder does no longer influence the illumination of the grating, but the imaging of the transmitted field as shown by comparison of Figs. 2(b), 2(e) to Figs. 2(c), 2(f).

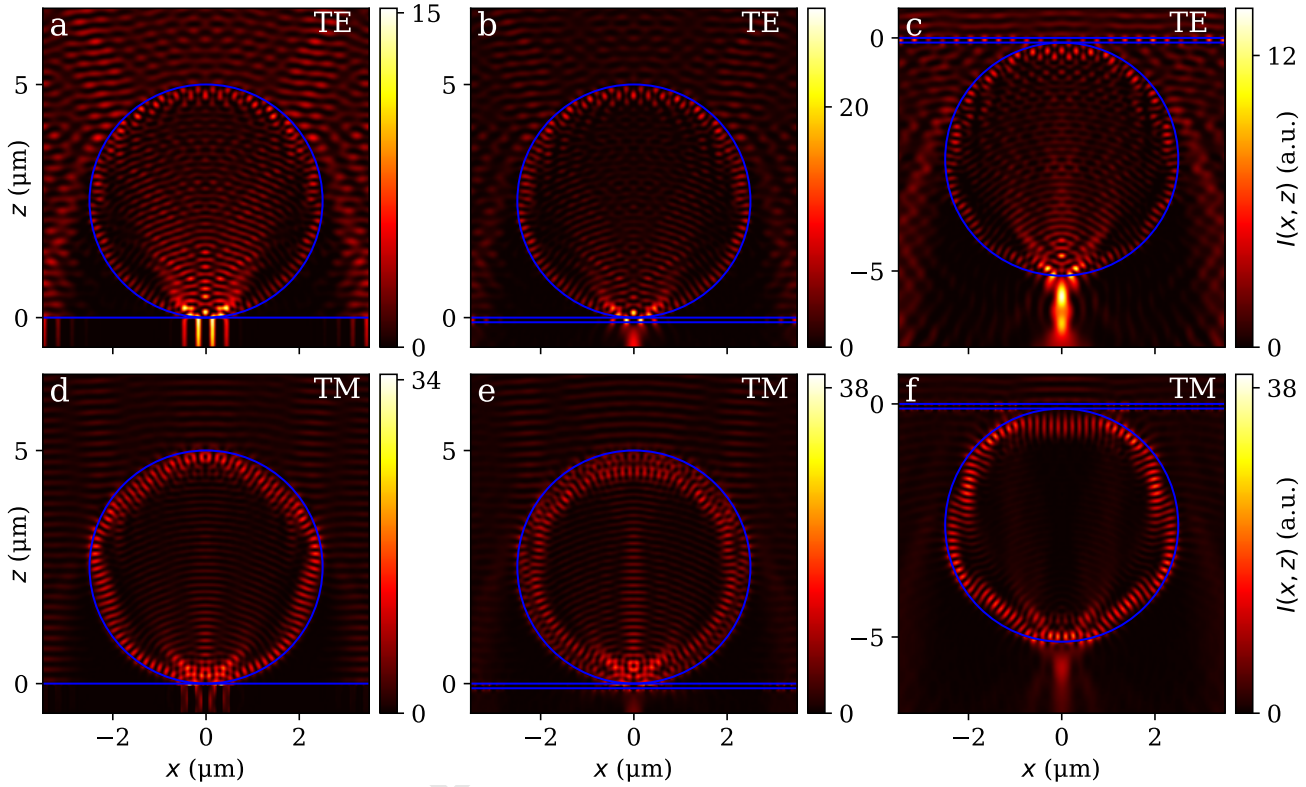

Figure 2. Extracts of simulated intensities obtained for a plane incident wave of unity amplitude with TE (a-c) and TM (d-f) polarization. The illumination wavelength, which is chosen to excite a WGM, is given by $\lambda = 448.975\,\text{nm}$ in case of TE and $\lambda = 442.951\,\text{nm}$ for TM polarization. In all figures, the illumination propagates from the top to the bottom and the intensity of the total field given by the sum of the incident and scattered field is shown. The profile is given by an axially infinitely extended amplitude grating placed below the cylinder (a,d), an amplitude grating of 100 nm axial extend placed below the cylinder (b,e), and an amplitude grating of 100 nm axial extend placed above the cylinder (c,f). All amplitude gratings have a period length of $l_x = 300\,\text{nm}$ and consist of glass and aluminum. The total geometry is assumed to be periodic with a period length of $L_x = 13.2\,\mu\text{m}$. The blue lines indicate the boundaries of the cylinder and the amplitude grating for better visibility.

3. RESULTS AND DISCUSSION

In order to calculate realistic image stacks obtained by a conventional microscope while the grating with the microcylinder on it moves through the focus of the objective lens, near-field calculations as exemplarily shown in Fig. 2 are repeated for several discrete incident angles within a cone, where the maximum angle of incidence is limited by the NA of the objective as described for interference microscopy by Pahl et al.[32] Figures 3(a) and 3(b) exemplarily show simulated intensity values obtained for NA = 0.9 with monochromatic TM polarized light of $\lambda = 440\,\text{nm}$. The results are calculated for $l_x = 300\,\text{nm}$ from an axially infinitely extended grating in reflection mode. Results are shown in the xz-plane, where x represents the lateral coordinate and z the axial coordinate. From Fig. 3(a) to 3(b) the grating is laterally shifted by half a period (180°) corresponding to an inversion of

the grating. As shown in the figures, the shift of the grating leads to intensity changes in the focal region of the cylinder (see horizontal lines). Note that the focal region of the field imaged by the cylinder is axially shifted compared to the virtual image plane. The focal region used for analyzes in this study is simply approximated by an area around the plane, where the focal plane is assumed to be. The exact focal plane can be analyzed e.g. by time reversal studies.[13,15] Further, it should be mentioned that due to the high NA system the grating can be resolved without a microcylinder as well. However, the simulation strategy is sufficient for an exemplary presentation of the method used to analyze the resolution limit.

Figure 3(c) displays the difference of the intensities shown in Figs. 3(a) and 3(b). As shown the grating is clearly visible in the focal area of the microcylinder (see horizontal lines). Cross sections of Figs. 3(a)-3(c) extracted from the axial position marked by the horizontal lines are shown in Fig. 3(d). The color of the plots correspond to the colors of the horizontal lines in Figs. 3(a)-3(c). Note that the intensities extracted from Figs. 3(a) and 3(b) are reduced by an offset for better visibility. Obviously, a phase shift of 180° appears between the red and green curves, which can be assigned to the phase shift of the grating according to Figs. 3(a) and 3(b). The difference ΔI between the intensities obtained for a grating and the laterally shifted one shows an enhanced oscillation due to the subtraction. If the grating would not be resolved by the microcylinder-assisted microscope setup, ΔI is expected to be zero. Hence, the standard deviation std(ΔI) of ΔI from zero can be used as an indicator of whether the grating is resolved or not.

In the following, std(ΔI) is calculated for different microscope setups explained in Sec. 2 depending on the period length l_x of the grating. Note that we consider only vertically incident plane wave illumination in the following resolution studies in order to reduce the computational burden. In a previous study[26] we demonstrated, that the resolution enhancement is independent of the NA of the objective lens and solely depends on the imaging properties of the microcylinder. The NA of the imaging objective lens is assumed to be 0.55. The illumination wavelengths are chosen similar to those used in Fig. 2 in order to excite WGMs.

Figure 3(e) displays simulated std values obtained for TM as well as TE polarized light depending on the period length l_x of the grating. Further, for TM polarized light, an axially infinitely (inf) extended as well as a grating of finite (fin) thickness $d = 100\,\text{nm}$ is considered. All std values are normalized by the value obtained from an infinitely thick grating of $l_x = 300\,\text{nm}$ with TM polarization. All three curves show the expected behavior and generally decrease with decreasing period length. This is in agreement with previous results obtained for interference microscopy.[26] Comparing the different polarization states, the resolution enhancement seems to be better for TM polarization. This result agrees with experimental observations published by Darafsheh et al.,[35] where a better contrast is achieved using TM polarized light in microsphere-assisted microscopy. Thus, in the following we mainly focus on TM polarization. In all three cases, the resolution is significantly increased compared to the lateral resolution for $l_x \approx 400\,\text{nm}$ according to the Abbe limit assuming NA = 0.55 for illumination and detection and air as the surrounding medium. Further, the resolution limit for TM polarized light seems to be below 180 nm. This result is in good agreement to the results obtained for interference microscopy[26] and can be explained with a local enhancement of the NA combined with a limited field of view through the cylinder. For an explanation of the effect of an improved resolution if only a few periods of the grating are in the field of view we refer to Lehmann et al.[36] Generally, the std values obtained for an infinitely extended grating and a grating of finite extent differ. Hence, internal reflections at the grating seem to affect the results. However, the resolution enhancement seems to be the same for both.

Figure 3(f) shows std values depending on the period length l_x if the microscope operates in transmission mode, where the microcylinder can be arranged in the illumination (ill) as well as the imaging (im) beam path. For both cases, the illumination is assumed to be TM polarized. For comparison, a result, where the cylinder consists of air corresponding to the absence of the microcylinder, is shown. As expected, without a microcylinder the grating is not resolved for the considered values of l_x and hence, std is zero.

However, for both transmission cases, the resolution seems to be enhanced compared to the reflection mode and below $l_x = 140\,\text{nm}$ in both configurations. Therefore, in case of transmission, the focused illumination as well as the imaging of evanescent waves seem to affect the resolution enhancement. This result is opposed to expectations concluded from simulation results obtained in previous studies for interferometric measurements of phase objects.[26] In order to get a deeper insight into the mechanisms leading to the resolution enhancement, Figs. 3(g) and 3(h) show simulated near-fields obtained for $l_x = 150\,\text{nm}$. Comparing Figs. 3(g) and 3(h), which differ only in the 180° of the grating above the cylinder, large differences in the fields obtained inside the cylinder

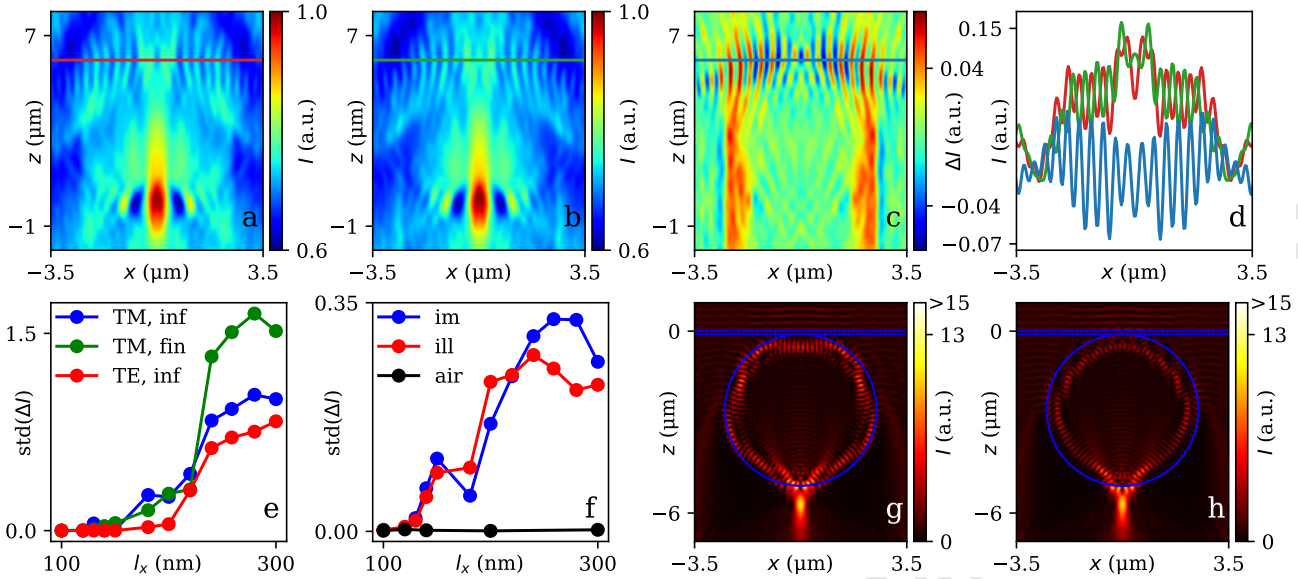

Figure 3. (a, b) Simulated intensities obtained from a grating (a) and its inverse (b) with $l_x = 300\,\text{nm}$ imaged by a microscope objective of NA = 0.9 used for illumination and imaging. The illumination light is assumed to be TM polarized with $\lambda = 440\,\text{nm}$. The difference of the intensities shown in (a) and (b) is displayed in (c). Cross sections along the colored lines marked in (a-c) are plotted in (d). The intensities obtained along the red and the green lines (a and b) are reduced by an offset for better visibility. (e) Standard deviation of intensities for a grating and its inverse depending on the period length l_x obtained for vertically incident light of different polarization in reflection mode assuming a detection NA of 0.55. The grating is considered to be infinitely extended in z-direction (inf) or of finite extend $d = 100\,\text{nm}$ (fin). (f) Standard deviation depending on l_x obtained in transmission mode for TM polarization, where the microcylinder is considered for illumination (ill) and imaging (im). The detection NA is assumed to be 0.55 as well. For comparison, the std value without a cylinder (implemented as a cylinder consisting of air and hence marked as air) is additionally shown. All std values are normalized by the std value obtained for TM polarized light from an infinitely thick grating with $l_x = 300\,\text{nm}$. (g, h) Simulated near-fields for $l_x = 150\,\text{nm}$ for original (g) and inverted (h) gratings in transmission mode with $d = 100\,\text{nm}$ and TM polarized light. The wavelengths for TE and TM are chosen to be similar to those of Fig. 2 for all subfigures of the bottom row.

appear. In both cases, a WGM is visible at the boundary of the cylinder. It should be noted that both intensities, which are calculated by the absolute square of the electric field neglecting other constant factors, are obtained for unity amplitude of the incident electric field. Hence, the field is significantly enhanced inside the cylinder in both figures. However, the shape and characteristics of the WGMs significantly differ. Therefore, the fields inside the cylinder and the shape of the excited WGM strongly depends on the phase of the grating above it. The obtained result is an indicator for the conversion of evanescent waves to propagating waves by microspheres and -cylinders as discussed in more detail by Zhou et al.[22] and Boudoukha et al.[19]

In comparison to the reflection mode, the effect of evanescent waves is expected to be enhanced in case of transmission since on the one hand the background field is expected to be significantly weakened and, on the other hand, further evanescent waves occur at the interface between glass and air. Nonetheless, also for reflection there seem to be slight contributions of the grating also for periods smaller than 180 nm. However, these contributions are strongly reduced compared to larger period lengths, what probably mainly follows from larger amplitudes of the reflected field compared to the transmitted field leading to increased contributions of other effects.

The resolution enhancement obtained using the cylinder in the illumination beam path seems to be similar to that obtained for the cylinder in the imaging beam path. This resolution enhancement can be caused by the illumination of a small spot similar to the confocal effect combined with the influence of evanescent waves occurring at the interfaces between the cylinder and the grating.

In sum, the resolution enhancement of MAM obtained using amplitude gratings is more significant than expected from previous studies[26] concluded from simulations of interference microscopy for phase gratings. Especially in case of transmission mode, the resolution improvement is larger due to the attenuated background field. The

conversion of evanescent waves to propagating waves seems to be the most likely reason. In case of the phase objects studied previously,[26] no appreciable influence of evanescent waves is expected. Instead, the local NA enhancement and a limited field of view turned out as the main effect for resolution enhancement. However, depending on the profile to be analyzed, the resolution is moreover improved by conversion of evanescent to propagating waves.

4. CONCLUSION

We present an FEM-based simulation model of microcylinder-assisted microscopy and show a way to analyze the resolution enhancement considering the imaging of grating profiles. Compared to previous studies, where phase gratings are imaged by interference microscopy, here we analyze the microcylinder-assisted microscopic imaging of amplitude gratings. The resolution enhancement obtained by these simulations is compared for setups operating in reflection and transmission mode. In case of transmission we further distinguish between placing the microcylinder in the illumination or the imaging beam path.

In both cases, reflection and transmission, the resolution is significantly enhanced compared to the fundamental resolution limit, which would be expected without microelement. In previous studies, for phase objects a local enhancement of the NA combined with a limited field of view is identified as the major reason leading to enhanced resolution. However, the resolution obtained in this study is also improved compared to the previously determined resolution limits for phase objects. The conversion of evanescent waves to propagating waves is identified to be the most likely reason for the additional resolution improvement, in particular seen in transmission mode imaging. In case of reflection, the improvement especially for extremely small period length seems to be less noticeable due to a larger background field compared to the evanescent field.

Hence, the resolution improvement achieved using microelements may have different reasons and strongly depends on the used measurement configuration as well as the object to be measured. However, it should be noted that the results presented in this study are based on a case study. Nonetheless, the results give an interesting insight in the complexity of effects supporting the resolution improvement in MAM and the presented model enables more detailed analyzes.

More detailed parameter studies as well as a quantitative comparison to measurement results are planed for future studies. Furthermore, the model can be easily extended to other microscopic imaging techniques such as confocal microscopy.

ACKNOWLEDGMENTS

The authors gratefully acknowledge the financial support of this research work by the DFG (German Research Foundation) [Grant no. LE 992/14-3, LE 992/15-1].

REFERENCES

[1] Singer, W., Totzeck, M., and Gross, H., [*Handbook of optical systems, volume 2: Physical image formation*], John Wiley & Sons, Weinheim (2006).

[2] Huszka, G. and Gijs, M. A. M., "Super-resolution optical imaging: A comparison," *Micro and Nano Engineering* **2**, 7–28 (2019).

[3] Mansfield, S. M. and Kino, G. S., "Solid immersion microscope," *Applied Physics Letters* **57**(24), 2615–2616 (1990).

[4] Mason, D. R., Jouravlev, M. V., and Kim, K. S., "Enhanced resolution beyond the abbe diffraction limit with wavelength-scale solid immersion lenses," *Optics Letters* **35**(12), 2007–2009 (2010).

[5] Wang, Z. B., Guo, W., Li, L., Luk'Yanchuk, B., Khan, A., Liu, Z., Chen, Z., and Hong, M., "Optical virtual imaging at 50 nm lateral resolution with a white-light nanoscope," *Nature Communications* **2**(1), 218 (2011).

[6] Li, L., Guo, W., Yan, Y., Lee, S., and Wang, T., "Label-free super-resolution imaging of adenoviruses by submerged microsphere optical nanoscopy," *Light: Science & Applications* **2**(9), e104 (2013).

[7] Darafsheh, A., *Optical super-resolution and periodical focusing effects by dielectric microspheres*, PhD thesis, The University of North Carolina at Charlotte, Charlotte (2013).

[8] Allen, K. W., Farahi, N., Li, Y., Limberopoulos, N., Walker, D., Urbas, A., and Astratov, V., "Overcoming the diffraction limit of imaging nanoplasmonic arrays by microspheres and microfibers," *Optics Express* **23**(19), 24484–24496 (2015).

[9] Wang, Z. B. and Luk'yanchuk, B., "Super-resolution imaging and microscopy by dielectric particle-lenses," in [*Label-Free Super-Resolution Microscopy*], Astratov, V. N., ed., 371–406, Springer, Cham (2019).

[10] Darafsheh, A., "Microsphere-assisted microscopy," *Journal of Applied Physics* **131**(3), 031102 (2022).

[11] Darafsheh, A., Limberopoulos, N., Derov, J., Walker Jr, D., and Astratov, V., "Advantages of microsphere-assisted super-resolution imaging technique over solid immersion lens and confocal microscopies," *Applied Physics Letters* **104**(6), 061117 (2014).

[12] Allen, K. W., Farahi, N., Li, Y., Limberopoulos, N., Walker Jr, D., Urbas, A., Liberman, V., and Astratov, V., "Super-resolution microscopy by movable thin-films with embedded microspheres: resolution analysis," *Annalen der Physik* **527**(7-8), 513–522 (2015).

[13] Kassamakov, I., Lecler, S., Nolvi, A., Leong-Hoï, A., Montgomery, P., and Hæggström, E., "3D super-resolution optical profiling using microsphere enhanced Mirau interferometry," *Scientific Reports* **7**(1), 3683 (2017).

[14] Montgomery, P. C., Lecler, S., Leong-Hoï, A., and Perrin, S., "High resolution surface metrology using microsphere-assisted interference microscopy," *Physica Status Solidi (a)* **216**(13), 1800761 (2019).

[15] Hüser, L. and Lehmann, P., "Microsphere-assisted interferometry with high numerical apertures for 3D topography measurements," *Applied Optics* **59**(6), 1695–1702 (2020).

[16] Yang, H., Moullan, N., Auwerx, J., and Gijs, M., "Super-resolution biological microscopy using virtual imaging by a microsphere nanoscope," *Small* **10**(9), 1712–1718 (2014).

[17] Darafsheh, A., Guardiola, C., Palovcak, A., Finlay, J., and Cárabe, A., "Optical super-resolution imaging by high-index microspheres embedded in elastomers," *Optics Letters* **40**(1), 5–8 (2015).

[18] Yang, S. L., Ye, Y., Shi, Q., and Zhang, J., "Converting evanescent waves into propagating waves: The super-resolution mechanism in microsphere-assisted microscopy," *The Journal of Physical Chemistry C* **124**(47), 25951–25956 (2020).

[19] Boudoukha, R., Perrin, S., Demagh, A., Montgomery, P., Demagh, N., and Lecler, S., "Near-to far-field coupling of evanescent waves by glass microspheres," *Photonics* **8**(3), 73 (2021).

[20] Yang, H., Trouillon, R., Huszka, G., and Gijs, M., "Super-resolution imaging of a dielectric microsphere is governed by the waist of its photonic nanojet," *Nano Letters* **16**(8), 4862–4870 (2016).

[21] Duan, Y. B., Barbastathis, G., and Zhang, B. L., "Classical imaging theory of a microlens with super-resolution," *Optics Letters* **38**(16), 2988–2990 (2013).

[22] Zhou, S., Deng, Y., Zhou, W., Yu, M., Urbach, H., and Wu, Y., "Effects of whispering gallery mode in microsphere super-resolution imaging," *Applied Physics B* **123**(9), 236 (2017).

[23] Wang, Z., Luk'yanchuk, B., Wu, B., Yan, B., Assel, A., Yaminsky, I., Yu, H., and Liu, L., "Optical super-resonances in dielectric microsphere particles," *Proc. SPIE* **12152**, 24–30 (2022).

[24] Minin, O. V. and Minin, I. V., "Optical phenomena in mesoscale dielectric particles," *Photonics* **8**(12), 591 (2021).

[25] Duocastella, M., Tantussi, F., Haddadpour, A., Zaccaria, R. P., Jacassi, A., Veronis, G., Diaspro, A., and Angelis, F. D., "Combination of scanning probe technology with photonic nanojets," *Scientific Reports* **7**(1), 3474 (2017).

[26] Pahl, T., Hüser, L., Hagemeier, S., and Lehmann, P., "Fem-based modeling of microsphere-enhanced interferometry," *Light: Advanced Manufacturing* **3**(4), 1–13 (2022).

[27] Darafsheh, A. and Abbasian, V., "Dielectric microspheres enhance microscopy resolution mainly due to increasing the effective numerical aperture," *Light: Science & Applications* **12**(1), 22 (2023).

[28] Maslov, A. V. and Astratov, V. N., "Resolution and reciprocity in microspherical nanoscopy: Point-spread function versus photonic nanojets," *Physical Review Applied* **11**(6), 064004 (2019).

[29] Sundaram, V. M. and Wen, S. B., "Analysis of deep sub-micron resolution in microsphere based imaging," *Applied Physics Letters* **105**(20), 204102 (2014).

[30] Hoang, T. H., Duan, Y., Chen, X., and Barbastathis, G., "Focusing and imaging in microsphere-based microscopy," *Optics Express* **23**(9), 12337–12353 (2015).

[31] Maslov, A., Jin, B., and Astratov, V., "Wave optics of imaging with contact ball lenses," *Scientific Reports* **13**(1), 6688 (2023).
[32] Pahl, T., Hagemeier, S., Künne, M., Yang, D., and Lehmann, P., "3D modeling of coherence scanning interferometry on 2D surfaces using FEM," *Optics Express* **28**(26), 39807–39826 (2020).
[33] Pahl, T., Hagemeier, S., Bischoff, J., Manske, E., and Lehmann, P., "Rigorous 3D modeling of confocal microscopy on 2D surface topographies," *Measurement Science and Technology* **32**(9), 094010 (2021).
[34] Cheng, F., Su, P.-H., Choi, J., Gwo, S., Li, X., and Shih, C.-K., "Epitaxial growth of atomically smooth aluminum on silicon and its intrinsic optical properties," *ACS Nano* **10**(11), 9852–9860 (2016).
[35] Darafsheh, A., Walsh, G. F., Dal Negro, L., and Astratov, V. N., "Optical super-resolution by high-index liquid-immersed microspheres," *Applied Physics Letters* **101**(14), 141128 (2012).
[36] Lehmann, P., Hüser, L., Stelter, A., and Kusserow, T., "Lateral resolution enhanced interference microscopy using virtual annular apertures," *Journal of Physics: Photonics* **5**(1), 015001 (2023).

T. Pahl, S. Hagemeier, L. Hüser, F. Rosenthal, P. Lehmann, "Simulative investigation of microcylinder-assisted microscopy in reflection and transmission mode" SPIE Proceedings 12619, Modeling Aspects in Optical Metrology IX, 126190K, (August 10, 2023).

https://doi.org/10.1117/12.2673443